

Machine learning and robust MPC for frequency regulation with heat pumps

Felix Bünning, Joseph Warrington, *Member, IEEE*, Philipp Heer, Roy S. Smith, *Fellow, IEEE*
and John Lygeros, *Fellow, IEEE*

Abstract—With the increased amount of volatile renewable energy sources connected to the electricity grid, there is an increased need for frequency regulation. On the demand side, frequency regulation services can be offered by buildings that are equipped with electric heating or cooling systems, by exploiting the thermal inertia of the building. Existing approaches for tapping into this potential typically rely on a first-principles building model, which in practice can be expensive to obtain and maintain. Here, we use the thermal inertia of a buffer storage instead, reducing the model of the building to a demand forecast. By combining a control scheme based on robust Model Predictive Control, with heating demand forecasting based on Artificial Neural Networks and online correction methods, we offer frequency regulation reserves and maintain user comfort with a system comprising a heat pump and a storage tank. We improve the exploitation of the small thermal capacity of buffer storage by using affine policies on uncertain variables. These are chosen optimally in advance, and modify the planned control sequence as the values of uncertain variables are discovered. In a three day experiment with a real multi-use building we show that the scheme is able to offer reserves and track a regulation signal while meeting the heating demand of the building. In additional numerical studies, we demonstrate that using affine policies significantly decreases the cost function and increases the amount of offered reserves and we investigate the suboptimality in comparison to an omniscient control system.

Index Terms—frequency regulation, robust Model Predictive Control, demand forecasting, building energy, affine policies

I. INTRODUCTION

The amount of renewable energy sources in the electricity grid is continuously increasing. As many of these sources are highly volatile, there is a growing need for frequency regulation [1]. Common strategies for frequency regulation are the deployment of fast-reacting power plants, for example gas or hydro-power, or the use of storage technologies, for example batteries. Besides such regulation on the supply side of the grid, frequency regulation on the demand side is possible through manipulation of controllable loads. This concept is often referred to as demand-side management.

This research project is financially supported by the Swiss Innovation Agency Innosuisse and is part of the Swiss Competence Center for Energy Research SCCER FEEB&D.

Joseph Warrington was and Roy S. Smith and John Lygeros are with the Automatic Control Laboratory, Department of Electrical Engineering and Information Technology, ETH Zürich, Switzerland. (email: joe.warrington@gmail.com; rsmith@control.ee.ethz.ch; jlygeros@ethz.ch)

Philipp Heer is with the Urban Energy Systems Laboratory, Swiss Federal Laboratories for Materials Science and Technology, Empa Dübendorf, Switzerland. (email: philipp.heer@empa.ch)

Felix Bünning is with both the Automatic Control Laboratory, ETH Zürich, and the Urban Energy Systems Laboratory, Empa Dübendorf. (email: buefelix@ethz.ch)

Possible candidates for demand-side management are buildings equipped with electric heating or cooling systems, such as heating, ventilation and air conditioning (HVAC) units, electric heaters and heat pumps [2]. Due to their thermal inertia, buildings are to an extent flexible when it comes to their heating and cooling requirements, hence their electricity consumption. By shifting their consumption in time they can therefore influence the grid frequency [3].

However, shifting electricity consumption can have an impact on occupant comfort as heating and cooling energy might not be available at the exact time when it is needed. There are different strategies to mitigate this influence. The authors of [4], [5], [6] develop and test control strategies for frequency regulation with heat pumps and HVAC units without explicitly enforcing comfort constraints and check only a-posteriori whether these were violated or not. References [7], [8] use heuristics based on weather forecasts and occupancy to limit the offered frequency reserve capacity to enforce comfort constraints. Many authors, for example [9], [10], [11], [12], use dynamic building models to exactly determine the influence of changed heating and cooling supply on room temperatures.

Combined with optimization in the frame of Model Predictive Control (MPC), such models can be used to maximize the offered frequency reserves while maintaining comfort constraints. References [13] and [14] develop Robust MPC schemes to provide day-ahead reserves for frequency regulation with commercial buildings and HVAC systems. Robust schemes ensure occupant comfort in the face of uncertainty in the regulation signal from the transmission system operator (TSO). In [15], [16] this approach is further developed and tested in a case study on a real small air-conditioned building.

The need for detailed models of the thermal dynamics of buildings is a potential drawback of MPC based approaches. Some authors argue that the cost of developing and maintaining first-principles building models could be holding back the wide-spread application of MPC in buildings in general [17], [18], which would also have implications on the use of MPC for building demand response as an extension to general MPC for building control [15]. While there is growing interest in more cost-effective data-driven and machine learning based building models, such models are so far only available for small and simple buildings [19], [18].

In contrast to this, data-driven heating and cooling demand forecasting for buildings or whole neighbourhoods and districts is a mature field, see for example the review of different methods in [20], [21], [22], [23], [24], [25], [26], [27]. Here,

inputs such as weather forecasts and calendar features, for example hour of the day or workday/non-workday, are used in combination with machine learning methods, often Artificial Neural Networks (ANN), to forecast heating or cooling energy consumption on different timescales. While [28], [29], [30], [31], [32] use different forms of single ANN for the prediction of heating and cooling demands of districts, [33], [34], [35], [36] do so for individual buildings. To mitigate the problem of high prediction variance between individual networks [37], [38] and [39] propose ensemble methods in the context of building demand prediction. As ensemble methods have the disadvantage of being computationally expensive, we have developed and validated correction methods based on online learning and error autocorrelation correction methods, which both decrease variance and increase accuracy, while avoiding the disadvantages of ensemble methods [40].

The problem of potentially expensive first-principles building models in the context of MPC for frequency regulation with electric building heating and cooling systems can be mitigated if demand and heating/cooling supply of the building are decoupled. This is the case if a buffer storage is placed between supply and demand. In this case, the thermal inertia of the buffer storage allows flexibility in heating and cooling energy production instead of the inertia of the building itself. The heating/cooling system and storage can in this case be modelled with first principles, which is tractable from an economic point of view as these are mass-produced products. The demand of the building can be modelled with any kind of forecasting method, such as the ANN methods mentioned above.

In this work, we combine the robust MPC for frequency regulation approach presented in [41] with the forecasting methods presented in [40] to offer frequency regulation reserves with a system comprising a ground-source heat pump and water buffer storage that meet the heating demand of a mixed-use building. The robust MPC approach is a further development of [15], which was adapted to this heating system. We apply affine policies, as discussed in [42] for reserve provision in power systems, which allows us to better exploit the available storage compared to standard open-loop MPC. We validate the methods in a three-day experiment on the real system and show that they are able to offer a substantial amount of regulation reserves and ensure good regulation signal tracking performance. Furthermore, we investigate optimality properties of the MPC solutions in two numerical experiments.

The remainder of the article is structured as follows. In Section II we introduce the reserve provision scheme and the system under consideration. In Section III we discuss the models for heat pump and storage as well as the prediction models with correction methods for the heating demand of buildings. We also describe the robust MPC based control scheme. In Section IV we present the experimental case study and its results. In Section V we describe the numerical case studies and discuss the suboptimality of the presented approach. We conclude in Section VI.

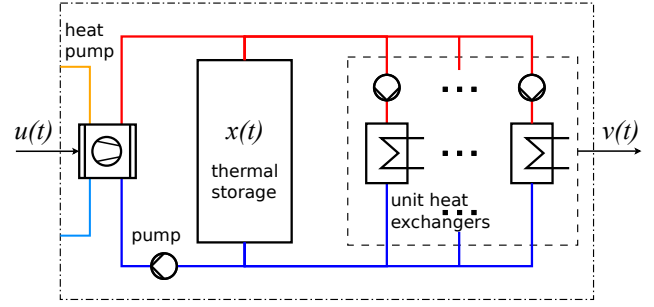


Fig. 1. Schematic of the system under consideration with heat pump, water storage tank and heat exchangers for individual apartments

II. PROBLEM STATEMENT

A. Reserve provision scheme

We assume a frequency regulation reserve scheme inspired by the regulation products offered by the U.S. transmission system operator PJM. In the considered scheme, the reserve provider communicates an offer $r \in \mathbb{R}^{96}$ of symmetric reserves to the TSO at midnight. The offer is made in 15-minute intervals for the next 24 hours. During the next day, when the offered reserves are due, the reserve provider can change their base consumption u_k^0 every timestep k (i.e. every 15 minutes). It should then track the electrical load

$$u_k(\tau) = u_k^0 + w(\tau)r_k, \quad (1)$$

where $w(\tau) \in [-1, 1]$ denotes the regulation signal which is updated every 2 seconds by the TSO, and r_k denotes the k^{th} element of the list of offered reserves r . u_k^0 and r_k are updated every 15 minutes, while $w(\tau)$ changes every 2 seconds. Thus, $u_k(\tau)$ also changes every 2 seconds.

The tracking performance is judged by a *composite performance score* monitored by the TSO, which consists of an *accuracy score*, which measures the correlation between the reserve signal and the system response, a *delay score* which measures the time delay between reserve signal and system response, and a *precision score* which measures the error between reserve signal and system response [43].

B. System under consideration

We consider the heating system for reserve provision shown in Figure 1. It consists of a vapour compression cycle heat pump, which is depicted on the left, and a water storage tank, which is depicted in the middle. The heat pump draws cold water from the bottom of the storage with the help of a pump, warms up the water by transferring heat from the refrigerant to the water inside the condenser, and feeds it back into the top of the storage. By varying the heat pump's electrical consumption, frequency regulation can be offered. On the right, individual pumps draw warm water from the top of the storage tank and pass it through heat exchangers, which supply individual rooms/units/apartments of the building with heat. The cold water is returned to the bottom of the tank. The models for each part of the system will be described in the following section.

III. METHODOLOGY

A. Models

The heat pump and water storage are modelled with first principles (physics based), while the heating demand of the building is modelled with the help of online corrected ANN. This is done, as heat pumps and storage tanks are mass-produced industrial products for which first principles models are relatively easy to develop, while buildings are generally different from each another and thus modelling the building demand with first principles would require significant effort for each building.

1) *Heat pump and storage model:* The heat pump, depicted on the left of Figure 1, generates high temperature heat $u_{th}(t)$ by using electricity $u(t)$ and ambient heat at a lower temperature level. Here, t denotes continuous time. The conversion efficiency between electrical energy and high temperature thermal energy is described by a coefficient of performance α_{COP} :

$$u_{th}(t) = \alpha_{COP} u(t) + e(t). \quad (2)$$

The error $e(t)$ is caused by the assumption of a constant COP. While in reality, $e(t)$ is dependent on several factors, such as ambient conditions and part load conditions, in the robust optimisation scheme introduced below we will simply model it by a rectangular uncertainty set. Note that equation (2) holds for any u_{th} and u , thus also for the discrete time instants used in the reserve scheme of (1).

Neglecting thermal losses, the average temperature $x(t)$ of the storage tank in Figure 1 is described by the energy balance

$$m c_p \frac{dx(t)}{dt} = u_{th}(t) - v(t) + \delta(t), \quad (3)$$

where m and c_p denote mass and specific heat capacity of the water respectively, $v(t)$ denotes the heating demand of the building, and $\delta(t)$ denotes the error between the forecast and the actual heating demand. Like the error $e(t)$ in (2), $\delta(t)$ will be modelled as a box-constrained uncertainty set for the robust optimization. Allowing mixing of different water layers in the storage, but assuming no swapping of temperature layers, the average temperature constitutes a lower bound for the water temperature in the top layer and an upper bound for the temperature in the lowest layer, which is sufficient for our control purpose. Moreover, model inaccuracies compared to a stratified tank model can also be captured by $\delta(t)$. Inserting equations (1) and (2) into equation (3) gives rise to the full linear description of the storage temperature:

$$m c_p \frac{dx(t)}{dt} = \alpha_{COP}(u_k^0 + w(\tau)r_k) + e(t) - v(t) + \delta(t). \quad (4)$$

2) *Building energy demand model:* The ANN forecasting approach with online correction methods for forecasting heating demands of buildings and districts has been presented in [40]. There, it was shown that the approach significantly reduces the variance in the prediction performance of the

ANN, while it also increases accuracy; in the study, the interquartile range of 100 different ANN reduces from 0.038 to 0.008, when correction methods are applied, while the average coefficient of determination improves from 0.818 to 0.885 in a real-life case study. For the sake of completeness, we reintroduce the methods here and adapt them to the forecasting task.

For the purposes of frequency reserve provision, a heating demand forecast for a building for the next 24 hours is made starting at midnight and afterwards every 15 minutes until the end of the day. The forecasting horizon thus decreases by 15 minutes with every forecast. Both training and validation data are assumed to be sampled at 15 minute time steps. The forecast is made with a feed-forward ANN, with inputs related to ambient conditions and time features. Two correction methods are applied in the online phase of the forecasting task (Figure 2).

The first correction method is based on the forecasting **error-autocorrelation**. The error \tilde{e} of the forecast conducted at the current time κ for forecasting interval k is estimated with

$$\tilde{e}_{\kappa,k} = e_{\kappa-1,1} R_{ee}(k, \mathcal{E}) \quad (5)$$

where

$$R_{ee}(l, \mathcal{E}) = \frac{\mathbb{E}[(\mathcal{E} - \mu)(\mathcal{E}_{+l} - \mu)]}{\sigma^2}. \quad (6)$$

Here, $e_{\kappa-1,1}$ denotes the difference between the first (15-minute) element of the last conducted forecast (at time $\kappa - 1$) and the actual measured heating demand. $R_{ee}(l, \mathcal{E})$ is the autocorrelation of the forecasting error, which is dependent on a time-lag l and the set of all past forecasting errors \mathcal{E} , including the training and testing data sets as well as the data gathered during online operation. \mathcal{E}_{+l} is the corresponding set shifted in time by l . The properties of the underlying stochastic process (expected value \mathbb{E} , mean μ and standard deviation σ) are empirically approximated based on the set \mathcal{E} .

The rationale behind the correction is based on the assumption that forecasting errors persist over time because the source for these errors also persist over time in a building; For example, opening a window will likely have an impact on the heating demand for a longer time period than a single 15-minute interval. The last measured forecasting error can thus be used to correct the next forecast.

The correction procedure is illustrated in Figure 2. A forecast is made at time κ based on the inputs f_κ . The previous forecast from time $\kappa - 1$ is compared to the actual measured heating demand, giving rise to $e_{\kappa-1,1}$. With all previously measured errors \mathcal{E} , stored in a database, \tilde{e}_κ can be calculated using equations (5) and (6). Adding \tilde{e}_κ to the uncorrected forecast gives rise to the corrected forecast v_κ , which will later be used as an input to the control scheme.

The second forecasting correction method is based on **on-line learning**: Instead of only training the ANN on a training set offline and using the ANN for predictions online, the ANN is retrained online every 24 hours on the basis of the data

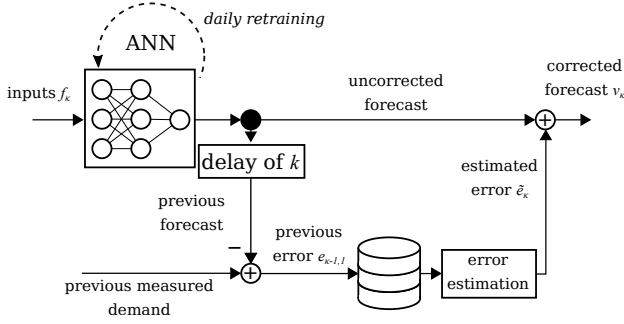


Fig. 2. Forecast correction on error-autocorrelation and online learning

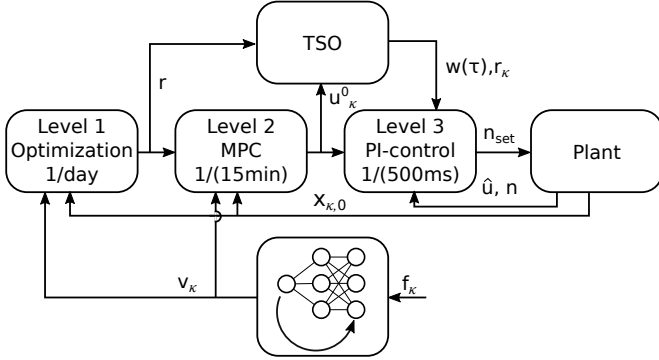


Fig. 3. Control scheme

gathered during the previous day. (This is symbolized by the dotted loop in Figure 2). By doing this, changes to the building that persist for longer than one day can be captured; such changes could include changing the set point of a thermostat for example.

For further details on the method and numerical results we refer to [40].

B. Control scheme

The models and demand forecasts developed in Section III-A are used in a 3-level control scheme for reserve provision inspired by [16]; see also [41] for an earlier implementation. The scheme is depicted in Figure 3. **Level 1** solves a robust optimization problem once every 24 hours at midnight. Based on the current storage tank temperature $x_{\kappa,0}$ and the heating demand forecast of the building v_k it determines the reserves r to be offered in 15 minute intervals, r_k , over the next 24 hours.¹ **Level 2** solves an optimisation problem similar to the one in Level 1 every 15 minutes during the day, with a shrinking horizon, from the current time to midnight. In this optimization problem, the values of the reserves r for the rest of the day are known, because they have been fixed by Level 1. The outputs of Level 2 are the nominal heat pump electrical power set points u_k^0 for each 15 minute interval of which the first one, $u_{\kappa,1}^0$, is passed on to Level 3. **Level 3** is a Proportional-Integral controller that controls the relative

rotational speed n of the heat pump's compressor to track the regulated heat pump's electricity consumption $u_\kappa(\tau)$.

For **Level 1**, equation (3) is discretized in time using exact discretization, leading to the state space model

$$x_{k+1} = \tilde{A}x_k + \tilde{B}(u_k - v_k + \delta_k). \quad (7)$$

By defining

$$A := \begin{pmatrix} \tilde{A} \\ \tilde{A}^2 \\ \vdots \\ \tilde{A}^N \end{pmatrix} \quad B := \begin{pmatrix} \tilde{B} & 0 & \dots & 0 \\ \tilde{A}\tilde{B} & \tilde{B} & \ddots & 0 \\ \vdots & \ddots & \ddots & \vdots \\ \tilde{A}^{N-1}\tilde{B} & \dots & \tilde{A}\tilde{B} & \tilde{B} \end{pmatrix}, \quad (8)$$

where N denotes the horizon, and redefining $x := [x_1, \dots, x_N]^T \in \mathbb{R}^N$, $u := [u_1, \dots, u_N]^T \in \mathbb{R}^N$, $v := [v_1, \dots, v_N]^T \in \mathbb{R}^N$, $\delta := [\delta_1, \dots, \delta_N]^T \in \mathbb{R}^N$ we describe the state trajectory by

$$x = Ax_0 + B(u - v + \delta), \quad (9)$$

where x_0 is the initial state of the system.

By vectorizing all remaining variables, the robust optimization problem in terms of the offered reserves r , the nominal heat pump electrical set points u^0 , and the heat pump on/off condition z , can be written as

$$\min_{r, x, u^0, u_{th}, \epsilon, z} f^{el}{}^\top u^0 - f^r{}^\top r + \lambda^\top \epsilon \quad (10a)$$

$$\text{subject to} \quad x = Ax_0 + B(u_{th} - v + \delta + e), \quad (10b)$$

$$u_{th} = \alpha_{COP}(u^0 + w \odot r), \quad (10c)$$

$$X_{\min} - \epsilon \leq x \leq X_{\max} + \epsilon, \quad (10d)$$

$$zU_{\min} \leq u^0 + w \odot r \leq zU_{\max}, \quad (10e)$$

$$z \in \mathbb{Z}_2^N, \quad (10f)$$

$$\epsilon \geq 0, \quad (10g)$$

$$\forall w \in W, \forall \delta \in \Delta, \forall e \in E. \quad (10h)$$

Here, f^{el} and f^r denote costs for electricity and benefits for offered reserves respectively. X_{\min} and X_{\max} describe temperature limits for the storage tank, defined by the lowest possible operating temperature for floor heating and the highest supply temperature of the heat pump. The slack variable $\epsilon \in \mathbb{R}^N$ ensures feasibility with respect to the storage temperature constraint and λ denotes the associated cost. The lower and upper electrical capacity limits of the heat pump are described by U_{\min} and U_{\max} , and $z \in \mathbb{Z}_2^N$ is a binary variable that determines if the heat pump is switched on or off. The symbol \odot denotes the operator for element-wise multiplication. All constraints have to hold for all realizations of uncertainties $w \in W, \delta \in \Delta, e \in E$.

Constraints (10c) and (10e) can be reformulated as linear constraints by making w a square diagonal matrix. Thus, problem (10) is a Mixed Integer Linear Program (MILP) that has to hold for the qualifier (10h). While W , Δ and E generally allow any convex sets, for box-constrained sets the robust optimization problem (10) can be reformulated as a tractable Mixed Integer Linear Program via *explicit maximization* [44].

¹The index $\kappa \in [1, 96]$ denotes the discrete time index, e.g. $\kappa = 1$ for midnight and $\kappa = 2$ for 00.15 a.m., while $k \in [1, N]$ denotes the index in the optimizations: for example, $u_{3,8}^0$ is the eighth element of the heat pump base consumption in the optimization conducted at time $\kappa = 3$ (00.30 a.m.).

The binary variable z forces u^0 and r , and thus u_{th} , to be zero if the electrical input to the heat pump does not exceed U_{min} . For the heating system this means that in case of low heating demand from the building, a hysteresis behaviour can be expected, where the heat pump changes between over-serving the demand and switching off. Potentially, there could be combinations of X_{min} , X_{max} , U_{min} and U_{max} where the heating demand could not be served, but this issue is captured by the slack variable ϵ .

In the case of low storage capacities, i.e. large \tilde{B} , corresponding to low mass of water, low X_{max} or high X_{min} , or large uncertainty in W , Δ , and E , the offered reserves r may become very small or, without the slack variable ϵ , the problem may even become infeasible. This is because the uncertainty induced in x by the action of w , δ , and e compounds along the horizon, as uncertainty at subsequent steps gets added to that of earlier steps through the integrator implicit in (10b) (see (3)). As a consequence, near the end of the horizon the uncertainty in x becomes large, leading to a violation of (10d).

This growth in uncertainty traces its origins to the fact that (10) addresses Level 1 in the control hierarchy of Figure 3, but does not contain any information about the actions of the lower levels. In reality, Level 2 and Level 3 will be executed repeatedly within the horizon of (10), adjusting the decisions of Level 1 to account for information that has become available in the meantime. This introduces feedback to the process, that will in practice limit the growth of the uncertainty.

In stochastic programming, information about this recourse process can be introduced by optimising over causal feedback policies instead of a sequence of open-loop decisions fixed at the beginning of the horizon. In this case, the optimisation problem for Level 1 encodes the fact that the system will react to uncertainties that are still unknown at the time (10) is solved, but will be revealed at the time the decision is implemented.

Unfortunately, as discussed in [42], optimizing over the set of all possible policies is intractable in general. To obtain a tractable optimisation problem, one can restrict the classes of causal policies considered. A common choice in this respect is the class of affine disturbance policies [45], [46]. For the uncertainties introduced by the regulation signal w , equation (10c) can be extended to

$$u_{th} = \alpha_{COP}(u^0 + w \odot r + D_w w), \quad (11)$$

where $D_w \in \mathbb{R}^{N \times N}$ is a strictly lower triangular matrix:

$$D_w := \begin{pmatrix} 0 & 0 & \cdots & 0 \\ [D_w]_{2,0} & 0 & \ddots & 0 \\ \vdots & \ddots & \ddots & 0 \\ [D_w]_{N,0} & \cdots & [D_w]_{N,N-1} & 0 \end{pmatrix}. \quad (12)$$

By making D_w a decision variable in the optimization problem, the uncertainty in u_{th} can be lowered, and thus also the uncertainty in x . Affine policies on the other uncertain variables δ and e can also be defined. Because δ and e appear together in (10b), a single lower triangular matrix can be used:

$$u_{th} = \alpha_{COP}(u^0 + w \odot r + D_w w + D_{\delta,e}(\delta + e)). \quad (13)$$

We note that the regulation signal that takes values in the interval $[-1, 1]$ is updated every 2 seconds, but the rest of the decision variables in (10) refer to quantities that are updated every 15 minutes. Therefore, when trying to meet the robust constraint (10c) the average value of w over a 15 minute interval (denoted by \bar{w} below) is more relevant than the instantaneous value. By collecting historical data, a second uncertainty set on the average of $w(\tau)$ can be created by integrating over 15-minute horizons and evaluating the distribution of these integrals (see [16]). As a result, the uncertainty set is decreased to $\bar{W} \subset W$ for constraint (10c). As the instantaneous electrical consumption needs to remain within operational limits at all times, $w \in W$ remains for constraint (10e).

The resulting optimization problem is

$$\min_{r, x, u^0, u_{th}, z, \tilde{z}, D_w, D_{\delta,e}, \epsilon} f^{el\top} u^0 - f^r\top r + \lambda\top \epsilon \quad (14a)$$

$$\text{subject to} \quad x = Ax_0 + B(u_{th} - v + \delta + e), \quad (14b)$$

$$u_{th} = \alpha_{COP}(u^0 + \bar{w} \odot r + D_w \bar{w} + D_{\delta,e}(\delta + e)), \quad (14c)$$

$$X_{min} - \epsilon \leq x \leq X_{max} + \epsilon, \quad (14d)$$

$$zU_{min} \leq u^0 + w \odot r + D_w \bar{w} + D_{\delta,e}(\delta + e) \leq zU_{max}, \quad (14e)$$

$$\tilde{z}R_{min} \leq r \leq \tilde{z}R_{max}, \quad (14f)$$

$$z, \tilde{z} \in \mathbb{Z}_2^N, \quad (14g)$$

$$\epsilon \geq 0, \quad (14h)$$

$$[D_w]_{i,j} = 0 \quad \forall j \geq i, \quad (14i)$$

$$[D_{\delta,e}]_{i,j} = 0 \quad \forall j \geq i, \quad (14j)$$

$$\forall w \in W, \forall \bar{w} \in \bar{W}, \forall \delta \in \Delta, \forall e \in E. \quad (14k)$$

The heat pump capacity constraint, now (14e), is adapted to ensure feasibility under the chosen policies. Note that, $[D_{\delta,e}]_{k,j}$ and $[D_w]_{k,j}$ (as well as u_k^0 and r_k) will be zero whenever $z_k = 0$. Moreover, as the results of [41] suggested that small reserves r lead to weak tracking performance (and low performance scores) because of large relative errors, a second binary variable \tilde{z} was added to impose a lower limit on r through constraint (14f). Problem (14) is still a MILP.

Controller **Level 2** is a MPC scheme with shrinking horizon. It can update u^0 , depending on updated measurements of initial conditions x_0 and updated forecasts v and uses an optimization problem similar to that of Level 1. The main difference is that r is now fixed, leading to



Fig. 4. NEST building at Empa in Switzerland. Open areas can accommodate future experimental units. Copyright: Zooey Braun - Stuttgart

$$\begin{aligned} \min_{x, u^0, u_{th}, z, D_w, D_{\delta, e}, \epsilon} \quad & f^{el\top} u^0 + \lambda^\top \epsilon \quad (15a) \\ \text{subject to} \quad & x = Ax_0 + B(u_{th} - v + \delta + e), \quad (15b) \end{aligned}$$

$$u_{th} = \alpha_{COP}(u^0 + \bar{w} \odot r + D_w \bar{w} + D_{\delta, e}(\delta + e)), \quad (15c)$$

$$X_{\min} - \epsilon \leq x \leq X_{\max} + \epsilon, \quad (15d)$$

$$\begin{aligned} zU_{\min} \leq u^0 + w \odot r + D_w \bar{w} \\ + D_{\delta, e}(\delta + e) \leq zU_{\max}, \quad (15e) \end{aligned}$$

$$z \in \mathbb{Z}_2^N, \quad (15f)$$

$$\epsilon \geq 0, \quad (15g)$$

$$[D_w]_{i,j} = 0 \quad \forall j \geq i, \quad (15h)$$

$$[D_{\delta, e}]_{i,j} = 0 \quad \forall j \geq i, \quad (15i)$$

$$\forall w \in W, \forall \bar{w} \in \bar{W}, \forall \delta \in \Delta, \forall e \in E. \quad (15j)$$

Level 3 is a discrete Proportional-Integral feedback controller, with proportional gain k_p and integral gain k_i , to track equation (1) with the heat pump. The controller output is the set point for the relative rotational compressor speed of the heat pump n_{set} . The controller input is the heat pump's measured electrical load \hat{u} . An anti-windup scheme is used in case the heat pump reaches its compressor speed limitations. The integration block of the controller is also bypassed if the difference between the set compressor speed n_{set} and the measured compressor speed n exceeds a limit. This is done because heat pumps usually have up and down ramping limits.

IV. EXPERIMENTAL CASE STUDY AND RESULTS

A. Configuration

We test the reserve scheme in a three-day experiment on a real system in the NEST building (Figure 4) at Empa, Switzerland. The building consists of individual residential, office and multi-use units that can be added and removed from the building backbone, as well as permanent office and meeting rooms. The individual units are connected to a central heating system with a supply temperature of 38 °C and a return



Fig. 5. Experimental set-up with heat pump and water storage tanks [41]

TABLE I
PARAMETERS FOR CONTROLLER LEVELS 1 AND 2

| | | |
|---|---|--|
| $N = 96,$ $\lambda = 5,$ $f^{el} = 1,$ $f^r = 1.5$ $R_{\min} = 0.4kW$ | $\alpha_{COP} = 3.53,$ $W = [-1, 1],$ $\bar{W} = [-0.25, 0.25],$ $U_{\min} = 8.2kW,$ $U_{\max} = 12.8kW,$ | $\bar{A} = 1,$ $\bar{B} = 0.0978 \frac{K}{kW},$ $X_{\min} = 28^\circ C,$ $X_{\max} = 38^\circ C,$ $E \oplus \Delta = [-4.0, 4.0] kW$ |
|---|---|--|

temperature of 28 °C via heat exchangers and are equipped with their own control systems considered to be unknown in the experiment.

The heating system (Figure 5) comprises a ground source heat pump, specifically the two-compressor model WP-WW-2NES 20.F4-2-1-S-P100 produced by Viessmann with a maximum thermal capacity of 100 kW, and a water buffer storage consisting of two 1100 litre Matica water tanks connected in series. Only the first compressor stage is used in the experiment. The system resembles the configuration described in Section II.

The control scheme configuration is as follows. The parameters for controller Levels 1 and 2 are shown in Table I. The cost-function related parameters λ , f^{el} , and f^r were chosen based on preliminary numerical studies to balance the trade-off between cost optimality and constraint violation. Compared to [41], we have increased the reserve benefit f^r to get richer r vectors to test the robustness of the controller. The values for α_{COP} , U_{\min} , U_{\max} and R_{\min} were set on the basis of preliminary heat pump experiments. The limits for W are properties of the used regulation signal RegD by PJM. The uncertainty set \bar{W} can be determined by analyzing historical regulation signals [16], \bar{A} follows from the assumption of no thermal losses, and \bar{B} is calculated on the basis of the tank volume and the specific heat capacity of water. In contrast to [41], where we chose the set boundaries based on historical measurement data from the building and the heat pump, we do not specify the uncertainty sets E (error from constant approximation of the COP) and Δ (error from demand forecast) separately, but instead define the Minkowski sum $E \oplus \Delta$, and shrink it compared to the original source. The initial value of the average tank temperature, x_0 , is determined by taking a weighted average of six temperature sensor measurements at different heights within the storage tank. To reduce wear on the heat pump, we introduce an additional constraint to Level 1, and require z_k to be constant during each thirty minute interval.

The proportional and integral gains, $k_p = 2.0$ and $k_i = 0.4$, of the PI controller in Level 3 were determined by first modelling and auto-tuning a first-order representation of the heat pump in Simulink®, and then manually adjusting the values after implementing the controller on the actual plant. The controller output limits for n_{set} are set to 20% and 50% of the relative compressor speed². The controller sampling time is 500 milliseconds and the maximum allowed difference between controller output n_{set} and measured compressor speed n before anti-windup activates is set to 2%. Moreover, as the heat pump is only fully controllable five minutes after switching it on, it is switched on five minutes early in the case that reserves are offered for the next 15-minute interval.

For the implementation of Levels 1 and 2 we use Matlab®. As all uncertain variables are box-constrained, the optimization problems become MILPs. These are written with YALMIP [44], which automatically derives robust counterparts, and are solved with CPLEX® 12.9. Each optimization is started five minutes before the decision is implemented, limiting the solver time to five minutes. This time is enough to solve the problem close to optimality in all cases.³ The best feasible solution is then implemented. The Level 3-controller is written in Python 3. The communication of the optimization results and the sensor measurements between Matlab and Python is facilitated via shared csv files. A Python OPC-UA client is used for the communication with sensors and actuators of the heat pump and the building.

The heating demand forecast is performed at midnight (for Level 1) and then every 15 minutes (for Level 2) with an ANN and the correction methods presented in Section III. The correction based on error-autocorrelation is applied with every new forecast, while the online retraining is done only at midnight. The ANN model uses as inputs the forecast ambient temperature (broadcast by MeteoSwiss and updated every 12 hours), the hour of the day (which is one hot encoded), the measured heating demand one day ago at the same time, the measured heating demand one week ago at the same time, and a binary variable that indicates whether it is a working or a non-working day. The ANN model is implemented in Python 3 with Keras [47]. It is a feed-forward network with two hidden layers and 8 nodes per hidden layer with Rectified Linear Units (ReLU) as activation functions. Just short of three years of historical data (sampled in 15 minute intervals) were used for training using the optimizer *adam* [48] with the standard learning rate of 0.001, a batch size of 1, and 10 epochs. This configuration corresponds to the one presented and validated in [40].

The experiment was conducted on three consecutive days from the 25th of February 2020, 11.45 am, to the 28th of February, 11.45 am. As a regulation signal, the RegD signal by PJM from the 27th of January 2019 was used for all three

days.⁴

B. Results

Figure 6 shows the results of the three day experiment. Note that the time axis is shifted by 11 hours and 45 minutes, to virtually let the experiment start at midnight. Plot (a) depicts the real heating demand of the NEST building in dashed blue, the forecast conducted at midnight for Level 1 in orange, and the forecasts for Level 2, which are conducted every 15 minutes, in transparent grey. The initial forecast (orange) predicts the trend of the heating demand well, confirming the results of [40]. The correction based on error-autocorrelation is visible, whenever the previous forecast significantly differs from the measured heating demand. This is the case at 00:00 at the beginning of the second day for example. At this point, the initial forecast of 23 kW (orange line) differs from the measured demand of 20 kW after one interval. The next corrected forecast at 00:15 (cyan line) therefore starts at 20 kW. The following corrected forecast at 00:30 (red line) starts at the measured demand of 16 kW. Both corrected forecasts merge back into the initial forecast over the course of the day because the error autocorrelation also decreases with time. It can also be seen that the experiment covers a range of heating demands from 10 kW, which is below the minimum thermal capacity of the heat pump, to 45 kW, which is close to the maximum capacity of the heat pump.

Plot (b) shows the reserves offered during the experiment. The reserves are either zero, or between 0.4 kW and 2.3 kW, which are the lower and upper limits. The upper limit is set as a constraint in the optimization problem, but is also a result of offering symmetric reserves and the electrical capacity of the heat pump being in the range of 8.2 to 12.8 kW. During the first day very little reserve is offered. This is for two reasons. First, the heat pump is frequently switched off because the demand is low. (See also plot (d) in Figure 6). In this case constraint (15e) forces the corresponding elements in D_w and $D_{\delta,e}$ to be zero, which means that recourse on uncertainties is no longer possible. Second, whenever the heat pump is on, it operates at the lower capacity limits, which for symmetric reserves results in offering no reserves. During the second and the third day of the experiment, reserves are offered during most of the 15 minute intervals. On day 1, 3.1% of the electricity consumed is flexible, on day 2 and 3, 14.9% and 19.1% are flexible respectively. The average of all three days is 13.4%.

Plot (c) shows the average storage temperature in solid black, the temperature constraints at 28 °C and 38 °C in dotted black and the six temperature measurements at different heights of the storage tank in transparent colors. The average temperature stays between the constraints for most of the time, except one 30 minute instance between 7.30 and 8.30 on day two. However, during this time the heating demand of the building could still be served, as the upper temperature layer in the storage tank (transparent blue) was above 28 °C at all times, which is a result of the average storage temperature

²The second compressor stage of the heat pump is activated if the relative speed exceeds the limit of 50%.

³We conducted preliminary numerical studies to investigate how the solution converges with time.

⁴This choice was made for convenience, as the signal starts and ends with a value of 1 and is thus continuous when repeated.

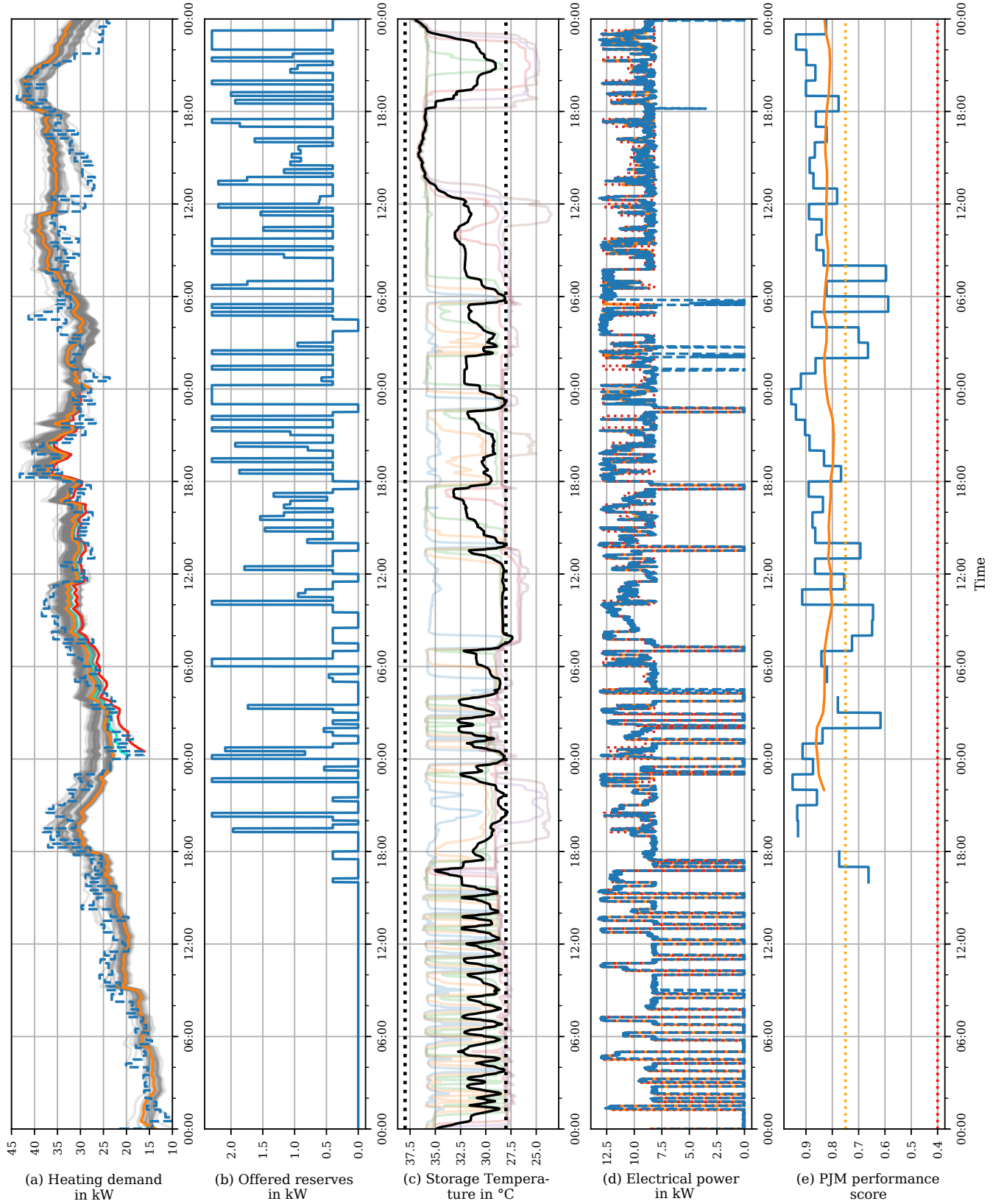


Fig. 6. Complete experimental results. (a): measured heating demand in dashed blue, daily forecast in orange, 15-minute forecasts in transparent grey, specifically mentioned forecasts in cyan and red, (b): offered reserves in blue, (c): average tank temperature in black, temperature constraints in dotted black, individual layer temperatures in transparent colours, (d): set point for electrical power in orange, measured electrical reserves in dashed blue, potential power range due to regulation signal in dotted red, (e): PJM performance score in blue, 20-hour moving average of performance score in orange, qualification limit in dotted orange, operation limit in dotted red.

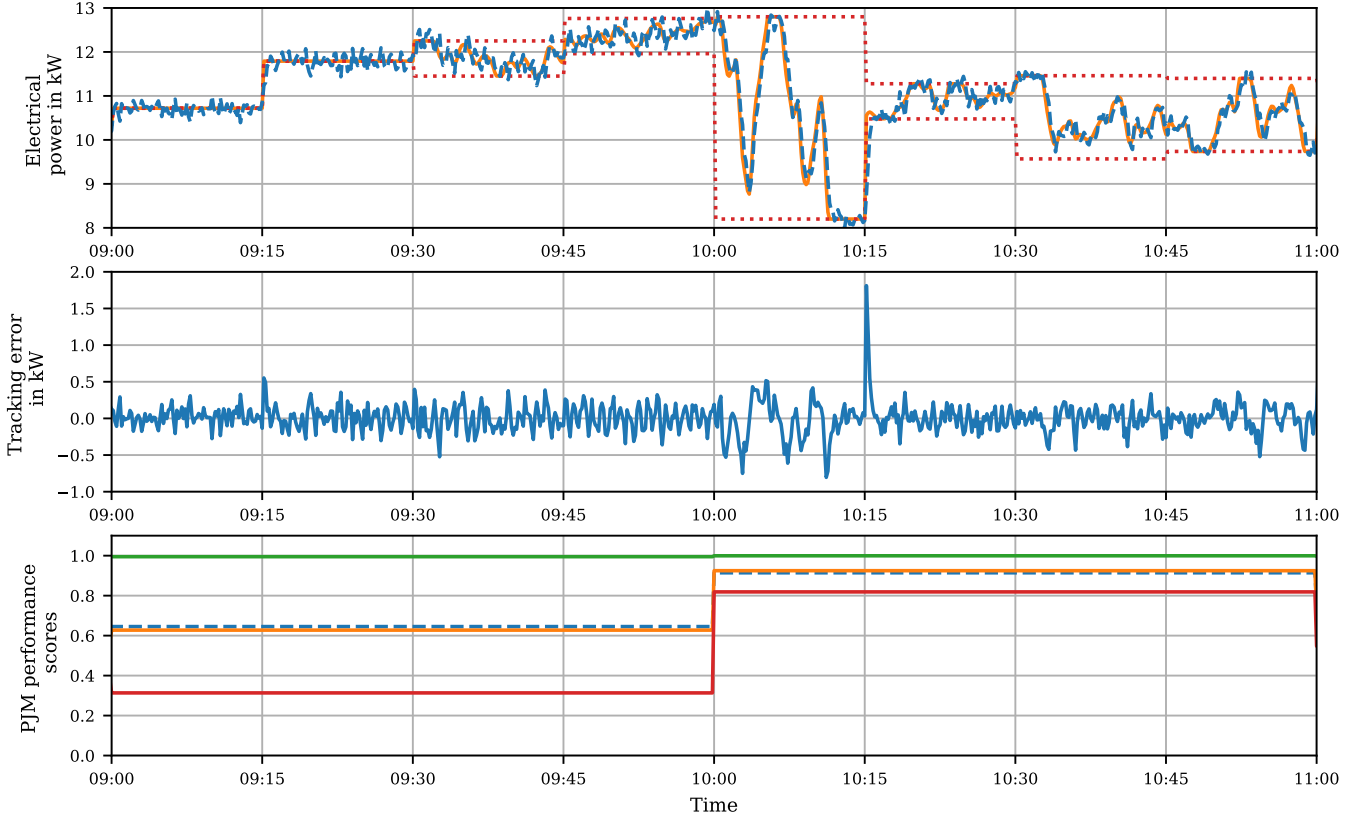


Fig. 7. Results tracking performance, Upper plot: set point for electrical power in orange, measured electrical reserves in dashed blue, potential power range due to regulation signal in dotted red, Middle plot: tracking error in blue, Lower plot: delay score in green, accuracy score in orange, precision score in red, composite score in dotted blue.

being a lower bound for the temperature of the top water layer in the storage tank. The average temperature stays relatively close to the lower constraint most of the time as a result of the optimization: unless needed for reserves, temperatures above the minimum mean unnecessary consumption of electricity. However, at times where the heating demand of the building is substantially overestimated by the initial demand forecast, the average storage temperature rises. This can be seen in the period between 12.00 and 18.00 on the third day.

Plot (d) of Figure 6 shows the set point for the electrical power of the heat pump in orange, the actual measured power of the heat pump in dashed blue and the possible range of the power due to the offered reserves in dotted red. As the results are difficult to read in this scale, an excerpt of this plot (9.00 to 11.00 of the second day) is shown in the upper plot of Figure 7. The effects of different sizes of offered reserves can be seen. From 9.00 to 9.30, where no reserves are offered, the heat pump does not exactly follow the set point; the resulting tracking error is also evident in the middle plot of Figure 7. There are two reasons for this tracking error. First, there is measurement noise of approximately ± 200 W. Second, the heat pump's internal controller only accepts integer set points for relative compressor speeds (e.g. 34% and 35%, but not 34.5%), which leads to a discontinuous control signal. After 9.30, a range of different reserves is offered, visible from the span between the red dotted lines. Visible from 10.00 to 10.15,

large reserves lead to bigger tracking errors because of the ramping limits of the heat pump. Large tracking errors also occur when large steps in the base set-point for the heat pump appear (at 10.15).

Despite these tracking errors, the performance score of the TSO PJM [43] is better when higher amounts of reserves are offered. This is shown in the lower plot of Figure 7. Here, the green line depicts the *delay score* (time delay between reserve signal and system response), the orange line depicts the *accuracy score* (correlation between the reserve signal and the system response), the red line depicts the *precision score* (error between reserve signal and system response) and the dashed blue line depicts the *composite score* (average of the three). The scores are averaged over one hour intervals and are normalized in the interval $[0, 1]$, with 1 being the best score. While the delay score is constantly high, both the accuracy score and especially the precision score become worse when the reserves offered are low, because the error relative to the offered reserves becomes large. Especially in the one-hour intervals where only small reserves are offered (or a combination of no reserves and small reserves), the composite performance score becomes low.

With respect to the whole experiment, this result is not problematic, as can be seen by going back to Figure 6. In plot (e), the composite performance score is shown in blue. The orange line depicts the 20-hour moving average

of the performance score. This is the metric used by PJM to judge whether a device or power plant is suitable for their reserve product. In the qualification phase, the limit for the performance score is 0.75 (dotted orange), while in the operational phase, the limit is lowered to 0.4 (dotted red). It can be seen that the performance score in this experiment is always well above both limits, confirming early results reported in [41].

V. NUMERICAL CASE STUDY AND RESULTS

To better understand the performance of the control scheme, we have further analyzed it in two numerical experiments.

A. Use of affine policies compared to open-loop MPC.

In the first numerical experiment, we compare the solution of Level 1 with affine policies (as presented in Section III) to a Level 1 scheme based on standard open-loop MPC without feedback policies for various constant heating demands v . The optimization problem for Level 1 for open-loop MPC is

$$\min_{x, r, u^0, u_{th}, z, \tilde{z}, \epsilon} f^{el\top} u^0 - f^{r\top} r + \lambda^\top \epsilon \quad (16a)$$

$$\text{subject to} \quad x = Ax_0 + B(u_{th} - v + \delta + e), \quad (16b)$$

$$u_{th} = \alpha_{COP}(u^0 + \bar{w} \odot r), \quad (16c)$$

$$X_{min} - \epsilon \leq x \leq X_{max} + \epsilon, \quad (16d)$$

$$zU_{min} \leq u^0 + w \odot r \leq zU_{max}, \quad (16e)$$

$$\tilde{z}R_{min} \leq r \leq \tilde{z}R_{max}, \quad (16f)$$

$$z, \tilde{z} \in \mathbb{Z}_2^N, \quad (16g)$$

$$\epsilon \geq 0, \quad (16h)$$

$$\forall w \in W, \forall \bar{w} \in \bar{W}, \forall \delta \in \Delta, \forall e \in E. \quad (16i)$$

The comparison is made for constant heating demands between 5 kW and 50 kW, in steps of 5 kW. All parameters for the optimization schemes are the same as in Section IV. Figure 8 and Figure 9 show the reserves offered and the cost functions (including the λ term) for both approaches. It can be seen in Figure 8 that without using feedback policies, the reserves offered are close to zero for most demands. This is due to the build-up of uncertainty in the state x (storage temperature) over the horizon of the optimization problem. In contrast, Level 1 with affine policies is able to offer reserves in most cases except when approaching the upper and lower capacity limits of the heat pump. From Figure 9 it can be seen that the value of the cost function is significantly lower when affine policies are used for all heating demands below 45 kW. Above 45 kW, there is no difference because the heat pump will always work at maximum capacity. We note however, that the played-out costs (with the MPC re-optimizing every 15 minutes) would have different results for both cases, which significantly depend on the uncertainty realizations.⁵

⁵While the played-out behaviour would certainly be an interesting result to study, the computational effort is immense: Assuming that 10000 uncertainty realizations are necessary to create a realistic overview of the effect of the uncertain variables, with an optimization time limit of five minutes, the simulation would take 164 years.

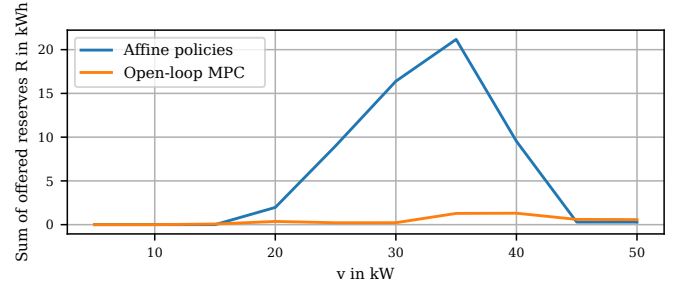


Fig. 8. Reserves offered in Level 1: affine policies vs. open-loop MPC

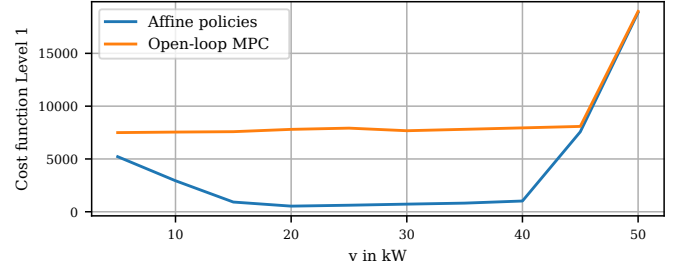


Fig. 9. Cost in Level 1: affine policies vs. open-loop MPC

B. Use of affine policies compared to a system with perfect knowledge.

In a second numerical experiment, we compare the performance of Level 1 using affine policies with an omniscient Level 1 solution that has perfect knowledge of all uncertainty realizations at the time of optimization. In this case, the optimization problem becomes

$$\min_{x, r, u^0, u_{th}, z, \tilde{z}, \epsilon} f^{el\top} u^0 - f^{r\top} r + \lambda^\top \epsilon \quad (17a)$$

$$\text{subject to} \quad x = Ax_0 + B(u_{th} - v + (\delta + e)), \quad (17b)$$

$$u_{th} = \alpha_{COP}(u^0 + \bar{w} \odot r), \quad (17c)$$

$$X_{min} - \epsilon \leq x \leq X_{max} + \epsilon, \quad (17d)$$

$$zU_{min} \leq u^0 + w_{min} \odot r, \quad (17e)$$

$$u^0 + w_{max} \odot r \leq zU_{max}, \quad (17f)$$

$$\tilde{z}R_{min} \leq r \leq \tilde{z}R_{max}, \quad (17g)$$

$$z, \tilde{z} \in \mathbb{Z}_2^N, \quad (17h)$$

$$\epsilon \geq 0, \quad (17i)$$

where $(\delta + e)$ is drawn from a uniform distribution with the same limits as the uncertainty set $E \oplus \Delta$, and w_{min} , w_{max} and \bar{w} are extracted from the regulation signal used (PJM RegD of 27th of January 2019). Here, w_{min} and w_{max} are the minimum and maximum value of the regulation signal that occurs during a 15 minute interval respectively; \bar{w} is the average of the interval.

The experiment is conducted for a constant heating demand v between 5 kW and 50 kW, in steps of 5 kW, with 10000 uncertainty realizations for each v . Optimization problem (17) is solved much faster than the robust counterpart of problem (15), requiring less than 5 seconds for convergence.

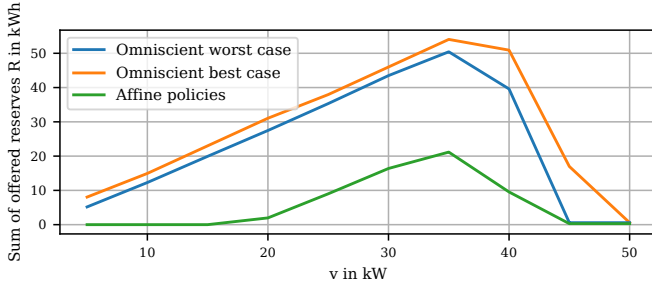


Fig. 10. Reserves offered in Level 1: affine policies vs. perfect knowledge

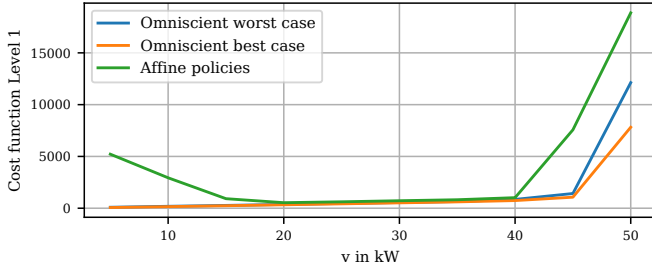


Fig. 11. Cost in Level 1: affine policies vs. perfect knowledge

Figure 10 shows the reserves offered for both cases for all different v . Here, the orange line denotes the best result achieved with the omniscient system with 10000 uncertainty realizations, while the blue line denotes the worst result. The green line shows the solution of Level 1 with affine policies. It can be seen that for all cases except $v = 45$ and 50 kW, the solutions with perfect knowledge of the uncertainties, offer significantly more reserves than the scheme with affine policies. The results for the cost function, depicted in Figure 11 for all v and depicted in Figure 12 for v between 15 and 40 kW, show that the scheme with perfect knowledge performs significantly better at very high and very low heating demands, which is due to avoiding the use of the slack variable ϵ . Also at intermediate demands, there is an offset between the cost functions of both schemes. This can be explained by the fact that the scheme with perfect knowledge is able to operate right at the storage temperature constraints (maximizing offered reserves or minimizing the base load), while the scheme with affine policies needs to stay at least $B(\Delta \oplus E)$ away from

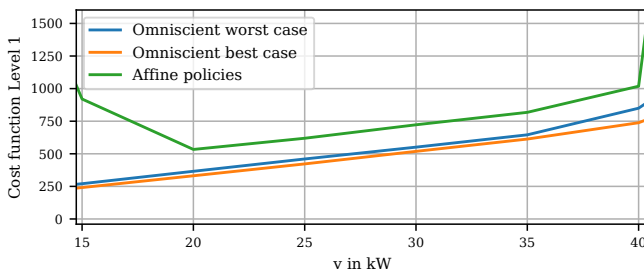


Fig. 12. Cost in Level 1: affine policies vs. perfect knowledge, in detail

the storage temperature constraint, even when no reserves are offered. This is the case because affine policies can only react to uncertainties in the timestep after their realization, unlike a system with perfect knowledge, which can plan ahead and can compensate for uncertainties before they are revealed. The larger optimality gap at 15 kW can again be explained by the fact that affine policies can only work when z is non-zero, which is often not the case for low heating demands.

VI. CONCLUSION

In this work, we have combined a three-level control scheme based on robust optimization with affine policies with heating demand forecasting based on ANN and online correction methods with the aim of offering frequency regulation reserves with heat pumps and water storage. The approach works without the necessity of a first principles building model and should thus reduce the modelling effort compared to including reserve provision in MPC building temperature control. The real life experiments on the heat pump and water storage in the NEST building with a varying heating demand have shown that the three-level control approach with affine policies on uncertain variables presented here is viable. The method allows the offering of frequency regulation reserves with a single variable speed heat pump and the performance of tracking the regulation signal is more than sufficient. On average, 13.4% of the consumed electricity is flexible as a result of the reserves offered. The heating demand forecasting approach with ANN and online correction methods gives predictions with high accuracy, such that the demand of the building can always be met. The numerical results further show that using affine policies on uncertainties significantly increases reserve provision and decreases cost when compared to using open-loop MPC. Nevertheless, the comparison with the omniscient optimisation indicates that there is still room for improvement. One possibility could be the use of more sophisticated policies (for example deflected linear [49], or piecewise linear [50] policies). However, due to causality constraints no policy can match the performance of an omniscient controller that knows the future. On a more practical note, a limitation of the approach presented here is that it can only work with variable speed heat pumps, which although becoming more common, are still relatively rare compared to fixed speed heat pumps. To offer reserves with fixed speed devices, a mechanism that pools heat pumps of many different buildings would be necessary in order to follow a continuous reserve signal.

ACKNOWLEDGMENT

We would like to thank Kristina Orehounig and Viktor Dorer for their valuable help and support. We are also grateful to Ahmed Aboudonia, Annika Eichler, Benjamin Flamm, Reto Fricker, Marc Hohmann, Benjamin Huber, Mathias Hudoba de Badyn, Andrea Ianelli, Mohammad Khosravi, Ralf Knechtle, Francesco Micheli, Anil Parsi and Sascha Stoller for fruitful discussions.

This research project is financially supported by the Swiss Innovation Agency Innosuisse and is part of the Swiss Competence Center for Energy Research SCCER FEEB&D.

REFERENCES

- [1] S. C. Johnson, D. J. Papageorgiou, D. S. Mallapragada, T. A. Deetjen, J. D. Rhodes, and M. E. Webber, "Evaluating rotational inertia as a component of grid reliability with high penetrations of variable renewable energy," *Energy*, vol. 180, pp. 258–271, Aug 2019.
- [2] H. Hao, B. M. Sanandaji, K. Poolla, and T. L. Vincent, "Potentials and economics of residential thermal loads providing regulation reserve," *Energy Policy*, vol. 79, pp. 115–126, Apr 2015.
- [3] D. Fischer and H. Madani, "On heat pumps in smart grids: A review," *Renewable and Sustainable Energy Reviews*, vol. 70, pp. 342–357, 2017.
- [4] J. Rominger, F. Kern, and H. Schmeck, "Provision of frequency containment reserve with an aggregate of air handling units," in *Computer Science - Research and Development*, vol. 33, no. 1-2. Springer Verlag, Feb 2018, pp. 215–221.
- [5] L. Romero Rodríguez, M. Brennenstuhl, M. Yadack, P. Boch, and U. Eicker, "Heuristic optimization of clusters of heat pumps: A simulation and case study of residential frequency reserve," *Applied Energy*, vol. 233–234, pp. 943–958, Jan 2019.
- [6] M. Maasoumy, J. Ortiz, D. Culler, and A. Sangiovanni-Vincentelli, "Flexibility of Commercial Building HVAC Fan as Ancillary Service for Smart Grid," in *Proceedings of Green Energy and Systems Conference 2013*, Nov 2013.
- [7] P. Zhao, G. P. Henze, S. Plamp, and V. J. Cushing, "Evaluation of commercial building HVAC systems as frequency regulation providers," *Energy and Buildings*, vol. 67, pp. 225–235, Dec 2013.
- [8] H. Wang, S. Wang, and K. Shan, "Experimental study on the dynamics, quality and impacts of using variable-speed pumps in buildings for frequency regulation of smart power grids," *Energy*, vol. 199, p. 117406, May 2020.
- [9] Y. J. Kim, L. K. Norford, and J. L. Kirtley, "Modeling and analysis of a variable speed heat pump for frequency regulation through direct load control," *IEEE Transactions on Power Systems*, vol. 30, no. 1, pp. 397–408, Jan 2015.
- [10] H. Hao, A. Kowli, Y. Lin, P. Barooah, and S. Meyn, "Ancillary service for the grid via control of commercial building HVAC systems," in *Proceedings of the American Control Conference*, 2013, pp. 467–472.
- [11] Y. Lin, P. Barooah, and S. P. Meyn, "Low-frequency power-grid ancillary services from commercial building HVAC systems," in *2013 IEEE International Conference on Smart Grid Communications, SmartGridComm 2013*, 2013, pp. 169–174.
- [12] M. Olama, T. Kuruganti, J. Nutaro, and J. Dong, "Coordination and Control of Building HVAC Systems to Provide Frequency Regulation to the Electric Grid," *Energies*, vol. 11, no. 7, p. 1852, Jul 2018.
- [13] X. Zhang, M. Kamgarpour, A. Georghiou, P. Goulart, and J. Lygeros, "Robust optimal control with adjustable uncertainty sets," *Automatica*, vol. 75, pp. 249–259, Jan 2017.
- [14] E. Vrettos, F. Oldewurtel, and G. Andersson, "Robust Energy-Constrained Frequency Reserves from Aggregations of Commercial Buildings," *IEEE Transactions on Power Systems*, vol. 31, no. 6, pp. 4272–4285, Nov 2016.
- [15] E. Vrettos, E. C. Kara, J. MacDonald, G. Andersson, and D. S. Callaway, "Experimental Demonstration of Frequency Regulation by Commercial Buildings-Part II: Results and Performance Evaluation," *IEEE Transactions on Smart Grid*, vol. 9, no. 4, pp. 3224–3234, Jul 2018.
- [16] —, "Experimental Demonstration of Frequency Regulation by Commercial Buildings-Part I: Modeling and Hierarchical Control Design," *IEEE Transactions on Smart Grid*, vol. 9, no. 4, pp. 3213–3223, Jul 2018.
- [17] D. Sturzenegger, D. Gyalistras, M. Morari, and R. S. Smith, "Model Predictive Climate Control of a Swiss Office Building: Implementation, Results, and CostBenefit Analysis," *IEEE Transactions on Control Systems Technology*, vol. 24, no. 1, pp. 1–12, Jan 2016.
- [18] A. Jain, F. Smarra, M. Behl, and R. Mangharam, "Data-Driven Model Predictive Control with Regression Trees An Application to Building Energy Management," *ACM Transactions on Cyber-Physical Systems*, vol. 2, no. 1, pp. 1–21, Jan 2018.
- [19] F. Bünning, B. Huber, P. Heer, A. Aboudonia, and J. Lygeros, "Experimental demonstration of data predictive control for energy optimization and thermal comfort in buildings," *Energy and Buildings*, vol. 211, p. 109792, Mar 2020.
- [20] M. A. Mat Daut, M. Y. Hassan, H. Abdullah, H. A. Rahman, M. P. Abdullah, and F. Hussin, "Building electrical energy consumption forecasting analysis using conventional and artificial intelligence methods: A review," pp. 1108–1118, Apr 2017.
- [21] H.-X. Zhao and F. Magoulès, "A review on the prediction of building energy consumption," *Renewable and Sustainable Energy Reviews*, vol. 16, pp. 3586–3592, 2012.
- [22] V. S. Harish and A. Kumar, "A review on modeling and simulation of building energy systems," *Renewable and Sustainable Energy Reviews*, vol. 56, pp. 1272–1292, 2016.
- [23] Z. Wang and R. S. Srinivasan, "A review of artificial intelligence based building energy use prediction: Contrasting the capabilities of single and ensemble prediction models," *Renewable and Sustainable Energy Reviews*, vol. 75, pp. 796–808, Aug 2017.
- [24] A. Fouquier, S. Robert, F. Suard, L. Stéphan, and A. Jay, "State of the art in building modelling and energy performances prediction: A review," *Renewable and Sustainable Energy Reviews*, vol. 23, pp. 272–288, 2013.
- [25] L. Suganthi and A. A. Samuel, "Energy models for demand forecasting A review," *Renewable and Sustainable Energy Reviews*, vol. 16, no. 2, pp. 1223–1240, Feb 2012.
- [26] K. Amasyali and N. M. El-Gohary, "A review of data-driven building energy consumption prediction studies," *Renewable and Sustainable Energy Reviews*, vol. 81, no. 1, pp. 1192–1205, Jan 2018.
- [27] T. Ahmad, H. Chen, Y. Guo, and J. Wang, "A comprehensive overview on the data driven and large scale based approaches for forecasting of building energy demand: A review," *Energy and Buildings*, vol. 165, pp. 301–320, Apr 2018.
- [28] K. Kato, M. Sakawa, Keiichi Ishimaru, S. Ushiro, and Toshihiro Shibano, "Heat load prediction through recurrent neural network in district heating and cooling systems," in *2008 IEEE International Conference on Systems, Man and Cybernetics*. IEEE, Oct 2008, pp. 1401–1406.
- [29] T. C. Park, U. S. Kim, L.-H. Kim, B. W. Jo, and Y. K. Yeo, "Heat consumption forecasting using partial least squares, artificial neural network and support vector regression techniques in district heating systems," *Korean Journal of Chemical Engineering*, vol. 27, no. 4, pp. 1063–1071, Jul 2010.
- [30] C. Johansson, M. Bergkvist, D. Geysen, O. D. Somer, N. Lavesson, and D. Vanhoudt, "Operational Demand Forecasting In District Heating Systems Using Ensembles Of Online Machine Learning Algorithms," *Energy Procedia*, vol. 116, pp. 208–216, Jun 2017.
- [31] G. Suryanarayana, J. Lago, D. Geysen, P. Aleksiejuk, and C. Johansson, "Thermal load forecasting in district heating networks using deep learning and advanced feature selection methods," *Energy*, vol. 157, pp. 141–149, 2018.
- [32] E. Saloux and J. A. Candanedo, "Forecasting District Heating Demand using Machine Learning Algorithms," in *Energy Procedia*, 2018.
- [33] S. Paudel, M. Elmtiri, W. L. Kling, O. L. Corre, and B. Lacarrière, "Pseudo dynamic transitional modeling of building heating energy demand using artificial neural network," *Energy and Buildings*, vol. 70, pp. 81–93, Feb 2014.
- [34] S. S. Kwok and E. W. Lee, "A study of the importance of occupancy to building cooling load in prediction by intelligent approach," *Energy Conversion and Management*, vol. 52, no. 7, pp. 2555–2564, Jul 2011.
- [35] M. Leung, N. C. Tse, L. Lai, and T. Chow, "The use of occupancy space electrical power demand in building cooling load prediction," *Energy and Buildings*, vol. 55, pp. 151–163, Dec 2012.
- [36] T. Mestekemper, G. Kauermann, and M. S. Smith, "A comparison of periodic autoregressive and dynamic factor models in intraday energy demand forecasting," *International Journal of Forecasting*, vol. 29, no. 1, pp. 1–12, Jan 2013.
- [37] R. Jovanović, A. A. Sretenović, and B. D. Živković, "Ensemble of various neural networks for prediction of heating energy consumption," *Energy and Buildings*, vol. 94, pp. 189–199, Jun 2015.
- [38] J. G. Jetcheva, M. Majidpour, and W. P. Chen, "Neural network model ensembles for building-level electricity load forecasts," *Energy and Buildings*, vol. 84, pp. 214–223, 2014.
- [39] M. De Felice and X. Yao, "Short-term load forecasting with neural network ensembles: A comparative study," *IEEE Computational Intelligence Magazine*, vol. 6, no. 3, pp. 47–56, Aug 2011.
- [40] F. Bünning, P. Heer, R. S. Smith, and J. Lygeros, "Improved day ahead heating demand forecasting by online correction methods," *Energy and Buildings*, vol. 211, p. 109821, 2020.
- [41] F. Bünning, J. Warrington, P. Heer, R. S. Smith, and J. Lygeros, "Frequency regulation with heat pumps using robust MPC with affine policies," presented at *IFAC World Congress 2020*, 2020.
- [42] J. Warrington, P. J. Goulart, S. Mariethoz, and M. Morari, "Robust reserve operation in power systems using affine policies," in *2012 IEEE 51st IEEE Conference on Decision and Control (CDC)*, Dec 2012, pp. 1111–1117.

- [43] PJM, “PJM Manual 12: Balancing Operations,” Tech. Rep., 2019.
- [44] J. Löfberg, “Automatic robust convex programming,” *Optimization Methods and Software*, vol. 27, no. 1, pp. 115–129, Feb 2012.
- [45] A. Ben-Tal, A. Goryashko, E. Guslitzer, and A. Nemirovski, “Adjustable robust solutions of uncertain linear programs,” *Mathematical Programming*, vol. 99, no. 2, pp. 351–376, Mar 2004.
- [46] P. J. Goulart, E. C. Kerrigan, and J. M. Maciejowski, “Optimization over state feedback policies for robust control with constraints,” *Automatica*, vol. 42, no. 4, pp. 523–533, Apr 2006.
- [47] F. Chollet, “Keras: The Python Deep Learning library,” *Astrophysics Source Code Library*, 2018.
- [48] D. Yun, H. Lee, and S. H. Choi, “A deep learning-based approach to non-intrusive objective speech intelligibility estimation,” *IEICE Transactions on Information and Systems*, vol. E101D, no. 4, pp. 1207–1208, Dec 2018.
- [49] X. Chen, M. Sim, P. Sun, and J. Zhang, “A linear decision-based approximation approach to stochastic programming,” *Operations Research*, vol. 56, no. 2, pp. 344–357, 2008.
- [50] A. Georghiou, W. Wiesemann, and D. Kuhn, “Generalized decision rule approximations for stochastic programming via liftings,” *Mathematical Programming*, vol. 152, no. 1-2, pp. 301–338, Aug 2015.